Dynamical properties of a hole in a Heisenberg antiferromagnet

Zhiping Liu and Efstratios Manousakis
Department of Physics, Center for Materials Research and Technology and Supercomputer Computations Research Institute, Florida State University, Tallahassee, Florida 32306
(Received 12 August 1991)

The t-J model in the large-t/J and low-doping limit is approximated by an effective Hamiltonian that treats spin degrees of freedom within the linear-spin-wave approximation and the hole-hopping term with a hole-spin interaction vertex that is linear in the spin-wave operators. The Dyson's equation for the single-hole Green's function is solved numerically on finite- but sufficiently large-size square lattices. Our calculation is based on an approximate equation for the hole motion that has been obtained using a self-consistent perturbation approach where crossing diagrams are neglected. We have studied the contribution of vertex corrections and found that the leading two-loop crossing diagram is exactly zero. Thus, the leading nonzero contribution to the proper self-energy from crossing diagrams is a three-loop correction. In two dimensions, it is possible to solve Dyson's equation numerically including these three-loop corrections. The results demonstrate that the contribution of such vertex corrections is indeed small. Our solution for the hole spectral function, obtained by neglecting such small contributions from vertex corrections, shows that most features describing the hole motion are in close agreement with the results of the exact diagonalization on the 4^2 lattice in the region of $J/t \leq 0.2$. The results obtained on sufficiently large-size lattices suggest that certain important features of the spectral function remain while others change due to finite-size effects. In particular, we find well-defined peaks above the lowest-energy peak that survive in the thermodynamic limit. We analyze these higher-energy peaks of the spectral functions and find that they can be understood as "string" excitations, which are created by the hole moving in a nearly linear potential.

I. INTRODUCTION

There is a consensus shared by many researchers that certain important magnetic properties of the undoped parent compounds of the superconducting cuprates can be understood by a spin-$\frac{1}{2}$ antiferromagnetic Heisenberg model on a two-dimensional (2D) square lattice.[1,2] Under light doping, which removes electrons, thereby producing mobile holes in the CuO_2 planes, these oxide compounds become superconducting. The interplay between antiferromagnetism and superconductivity may be important in the theoretical understanding of the superconducting mechanism. A simple model that combines an antiferromagnetic exchange interaction between spins and a hopping matrix element to describe hole conductivity is given as

$$\hat{H}_{t\text{-}J} = -t \sum_{<i,j>\sigma} (\bar{c}^{\dagger}_{i,\sigma}\bar{c}_{j,\sigma} + \text{H.c.}) + \sum_{<i,j>} [J_z S^z_i S^z_j + \frac{1}{2} J_{\perp}(S^+_i S^-_j + S^-_i S^+_j)], \quad (1)$$

where $< ij >$ denotes pairs of nearest-neighbor sites, and $\bar{c}_{i,\sigma}$ is the constrained hole creation operator defined as $\bar{c}_{i,\sigma} = c_{i,\sigma}(1 - n_{i,\bar{\sigma}})$, while $c_{i,\sigma}$ denotes the annihilation operator for an electron with spin σ on the lattice site i, and $n_{i,\bar{\sigma}} = c^{\dagger}_{i,\bar{\sigma}} c_{i,\bar{\sigma}}$ is the number operator with a spin opposite to σ. The isotropic case $J_z = J_{\perp} = J$ will be the subject of our studies. This model, now known as the "t-J model," has received significant attention by various authors because it can be derived from more realistic models that account for the detailed chemical structure of the copper oxide planes.[3]

Considerable attempts have been made to study the 2D t-J model in the presence of a single hole, using both analytical and numerical techniques. Green's-function techniques,[4–7] variational approaches,[8–10] and exact diagonalization studies[11–13] as well as other studies[14] have provided useful information about certain features of the single-hole dispersion relation and the spectral function. Although it is commonly believed by many investigators[7–11] that there is a well-defined quasihole ground state whose momentum is $\mathbf{k} = (\pm\frac{\pi}{2}, \pm\frac{\pi}{2})$, some dynamical properties such as hole lifetime, effective mass, etc., remain controversial. These important properties need to be well understood, not only because of their possible connection to the mechanism of high-temperature superconductivity, but also because of the fact that the t-J model is one of the simplest theoretical models describing the physics of strongly correlated electronic systems.

The motion of a hole in a classical Néel state was studied in detail by Brinkman and Rice using the retraceable path approximation.[4] They found that as a hole hops it ruins antiferromagnetically aligned spin configurations and produces a string of flipped spins along its path. Thus, they argued that only those paths that return to the origin leaving the spin configuration unchanged are important in calculating the hole Green's function. In

the atomic limit of the Hubbard model, they found that the hole motion is incoherent. In the case of small but finite coupling J_z and $J_\perp = 0$ (i.e., in the t-J_z model), a string of overturned spins costs an energy proportional to the length of the path and the hole can be treated as if it was a particle moving in a linear potential.[8] Bound states with discrete energy levels proportional to $t(J_z/t)^{2/3}$ are solutions to this problem. Hence, a single hole seems to be tied to its original site by a string. On the other hand, there is another hole-hopping mechanism proposed by Trugman,[10] which does not cost string energy. Namely, if the hole moves around a closed path two steps less than two full circuits without self-intersecting, it will find itself translated either to a next-nearest-neighbor site or to a third-nearest-neighbor site with the background spins undisturbed. The hole does not have an infinite effective mass in this case but has a finite mobility.

Quantum spin fluctuations due to the Heisenberg antiferromagnetic exchange interaction are expected to erase part of the "string" by flipping pairs of spins spontaneously and make the holes mobile. To obtain information about hole dynamical properties one can study the hole propagator in a Heisenberg antiferromagnet. Several studies[7,10–12] have confirmed that the hole spectral function for certain momentum states has a sharp peak as a function of the energy at the bottom of the hole spectrum, which means that a coherent excitation exists, and a quasiparticle description is valid. The positions of these quasiparticle peaks as a function of momentum determine the hole band and thereby determine the effective quasiparticle mass. Recent studies of the hole spectral functions suggest that strings may not be completely erased by quantum spin fluctuations.[10,11] In particular, it has been found that some fine structures above the quasiparticle peak in the hole spectral function exist and are probably related to the string states. In an exact diagonalization study, Dagotto *et al.*[11] identified the peaks above the quasiparticle peak as string excitations by fitting the peak positions as a power-law function of J/t. These results need to be examined further considering the fact that they have been obtained on a rather small lattice (4^2).

In this paper we present numerical solutions for the Dyson's equation of a single-hole Green's function on a square lattice using the approach of Schmitt-Rink, Varma, and Ruckenstein[6] (SVR) and Kane, Lee, and Read[7] (KLR). We assume that the ground state for the spins at half filling is described by the spin-wave theory; therefore the antiferromagnetic long-range order exists, and the spin excitations are spin waves. We show that the contribution from the two-loop crossing diagram is exactly zero so that the leading nonzero vertex correction to the hole Green's function is given by a three-loop crossing diagram. We solve Dyson's equation by including the leading nonzero vertex corrections and find no significant changes in the spectral functions by comparing with the results calculated without vertex corrections in the region of small J/t ($J/t \leq 0.3$). We compare the hole spectral function calculated without contributions from vertex corrections with the exact results obtained on a 4^2 lattice by Dagotto *et al.*[11] and find that they are in close agreement in the small-J/t region. Our method can be applied to much larger size lattices and thus it allows us to study finite-size effects. Our numerical results on the hole spectrum have been obtained without the need for the additional "dominant-pole approximation" used by KLR, who found that the spectral function contains a quasiparticle peak and an incoherent part of spin excitations above it. However, we find that there exist other well-defined peaks in the spectral function, beyond the lowest-energy peak, which survive in the thermodynamic limit. Our analysis indicates that these peaks correspond to string excitations. Within the t-J_z model these are well-defined excitations, and they arise from the existence of a linear potential seen by the hole as it moves away from its original position. In the t-J model, these peaks acquire a width (i.e., finite lifetime) due to the effects of quantum spin fluctuations on the linear potential seen by the hole. Our results are in agreement with the conclusions of Trugman[10] and Dagotto *et al.*,[11] that string excitations of a mobile hole are not destroyed by the quantum spin fluctuations caused by the Heisenberg exchange interaction for small J/t.

The paper is organized as follows. In Sec. II, we give the derivations for the effective Hamiltonian and Dyson's equation. In Sec. III, we study vertex corrections, to the hole spectral function. In Sec. IV, we compare our results with the exact results obtained on a 4^2 lattice. In Sec. V, we analyze our results obtained on much larger size lattices, and we discuss finite-size effects and the string excitations. Finally, in Sec. VI, we draw conclusions.

Part of our results were first reported in a Rapid Communication.[15] The paper presented here gives more details about the calculation and further results as well as studies of the contribution of higher-order vertex corrections and an analysis of the peaks in the spectral function caused by string excitations.

Upon the completion of this work, we became aware of one paper by Marsiglio *et al.*[16] and another by Martínez *et al.*[17] who have also solved the single-hole Dyson's equation numerically. However, we have also studied the contribution of vertex corrections, and we also find that there are peaks due to string excitations that survive in the thermodynamic limit. In particular, we have shown that the two-loop crossing diagram is exactly zero and have also computed the hole spectral function including the three-loop crossing diagrams self-consistently. In addition, we have thoroughly explored the higher-energy peaks in the spectral function, which, as we show, survive in the thermodynamic limit and correspond to higher-energy string excitations.

II. FORMULATION

Following the work of SVR and KLR, we treat the J term of the Hamiltonian (1) using the linear-spin-wave approximation.[18] We use the Holstein-Primakoff transformation,

$$S_i^\dagger = \sqrt{2S}a_i, \quad S_i^z = S - a_i^\dagger a_i; \quad i \in \uparrow, \tag{2}$$

$$S_i^\dagger = \sqrt{2S}b_i^\dagger, \quad S_i^z = -S + b_i^\dagger b_i; \quad i \in \downarrow, \tag{3}$$

where our notation $i \in \uparrow$ ($i \in \downarrow$) means that the site i is on the up sublattice (down sublattice). We define the following Fourier transformations,

$$a_{\mathbf{k}} = \sqrt{\frac{2}{N}} \sum_{i \in \uparrow} e^{i\mathbf{k}\cdot\mathbf{r}_i} a_i, \quad b_{\mathbf{k}} = \sqrt{\frac{2}{N}} \sum_{i \in \downarrow} e^{i\mathbf{k}\cdot\mathbf{r}_i} b_i. \quad (4)$$

Introducing the Bogoliubov canonical transformation,

$$a_{\mathbf{k}} = v_k \alpha_{\mathbf{k}} + u_k \beta^\dagger_{\mathbf{k}}, \quad b_{-\mathbf{k}} = v_k \beta_{\mathbf{k}} + u_k \alpha^\dagger_{\mathbf{k}}, \quad (5)$$

we write the Heisenberg term of the t-J Hamiltonian as

$$\hat{H}_J = E_0 + \sum_{\mathbf{k}} \Omega_{\mathbf{k}} (\alpha^\dagger_{\mathbf{k}} \alpha_{\mathbf{k}} + \beta^\dagger_{\mathbf{k}} \beta_{\mathbf{k}}), \quad (6)$$

where N is the total number of sites, E_0 is the spin wave ground state energy and $\Omega_{\mathbf{k}} = JzS\sqrt{1-\gamma^2_{\mathbf{k}}}$ is the spin wave dispersion with z being the number of the nearest neighbors. In this paper we are only interested in the spin-$\frac{1}{2}$ case. The summation over $\mathbf{k}$ is restricted inside the reciprocal Brillouin zone of one sublattice. The transformation coefficients are given by

$$u_{\mathbf{k}} = \left(\frac{1}{2}[(1-\gamma^2_{\mathbf{k}})^{-1/2} + 1]\right)^{1/2}, \quad (7)$$

$$v_{\mathbf{k}} = -\mathrm{sgn}(\gamma_{\mathbf{k}}) \left(\frac{1}{2}[(1-\gamma^2_{\mathbf{k}})^{-1/2} - 1]\right)^{1/2}, \quad (8)$$

where $\gamma_{\mathbf{k}} = \sum_{\delta} e^{i\mathbf{k}\cdot\delta}/z$ and δ is a unit vector connecting z nearest neighbors.

We define the hole operators, which obey Fermi statistics such that $h_i = c^\dagger_{i\uparrow}$ on the $\uparrow$ sublattice and $f_i = c^\dagger_{i\downarrow}$ on the $\downarrow$ sublattice. Hence the other electron operators can be written as

$$c_{i\downarrow} = h^\dagger_i a_i, \quad i \in \uparrow; \qquad c_{i\uparrow} = f^\dagger_i b_i, \quad i \in \downarrow. \quad (9)$$

With the constraint of no double occupancy, the hopping Hamiltonian takes the form

$$\hat{H}_t = t \sum_{<i\in\uparrow, j\in\downarrow>} [(1-a^\dagger_i a_i) h^\dagger_i b^\dagger_j f_j + h^\dagger_i f_j a_i (1-b^\dagger_j b_j) + \mathrm{H.c.}] + t \sum_{<i\in\downarrow, j\in\uparrow>} [(1-b^\dagger_i b_i) f^\dagger_i a^\dagger_j h_j + f^\dagger_i h_j b_i (1-a^\dagger_j a_j) + \mathrm{H.c.}], \quad (10)$$

where $h^\dagger_i$ and $f^\dagger_j$ are spinless fermion operators, which create holes on $\uparrow$ and $\downarrow$ sublattices, respectively. In the linear spin-wave approximation one keeps up to quadratic terms in the hard-core boson operators in both the Heisenberg and hopping terms of Eq. (1). In this approximation the hole spin-wave coupling term is

$$\hat{H}_t \simeq \sum_{\mathbf{k},\mathbf{q}} \{ h^\dagger_{\mathbf{k}} f_{\mathbf{k}-\mathbf{q}} [g(\mathbf{k},\mathbf{q})\alpha_{\mathbf{q}} + g(\mathbf{k}-\mathbf{q},-\mathbf{q})\beta^\dagger_{-\mathbf{q}}] + f^\dagger_{\mathbf{k}} h_{\mathbf{k}-\mathbf{q}} [g(\mathbf{k}-\mathbf{q},-\mathbf{q})\alpha^\dagger_{-\mathbf{q}} + g(\mathbf{k},\mathbf{q})\beta_{\mathbf{q}}]\} + \mathrm{H.c.}, \quad (11)$$

where,

$$g(\mathbf{k},\mathbf{q}) = tz\sqrt{\frac{2}{N}}(u_q \gamma_{\mathbf{k}-\mathbf{q}} + v_q \gamma_{\mathbf{k}}). \quad (12)$$

Given this effective Hamiltonian, which is composed of parts (6) and (11), we can calculate the Green's function of a single hole. Although there are two types of holes created by $f^\dagger$ and $h^\dagger$, respectively, it is sufficient to consider only the hole propagator of one type. For example, the Green's function of h-type hole is defined as

$$G(\mathbf{k},t) = -i\langle\psi_0|T[h_{\mathbf{k}}(t) h^\dagger_{\mathbf{k}}(0)]|\psi_0\rangle, \quad (13)$$

where ψ_0 is the ground state of the Heisenberg model in the half filling and T is a time-order operator. In the limit $J \ll t$, using a self-consistent perturbation approach where only noncrossing diagrams are summed, one obtains the following Dyson's equation for the hole propagator:

$$G(\mathbf{k},\omega) = \frac{1}{\omega - \sum_{\mathbf{q}} g^2(\mathbf{k},\mathbf{q}) G(\mathbf{k}-\mathbf{q}, \omega - \Omega_{\mathbf{q}})}. \quad (14)$$

In this approximation, the vertex, which couples the hole to the spin waves, is neglected. We will show in the next section that the leading-order one-loop vertex corrections (i.e., two loops in the self-energy Σ) are exactly zero and the two-loop vertex corrections (i.e., three loops in Σ) are small in the large t limit. Equation (14) has been numerically solved in one dimension by SVR.[6] The 2D case has been studied analytically by KLR[7] in the various limits. They used the so-called dominant-pole approximation, which assumes that the hole spectrum is incoherent above the quasiparticle peak. In this paper, we give the numerical solutions obtained by iterating Eq. (14) on finite clusters of size $N = L \times L$ starting from

$$G^{(0)}(\mathbf{k},\omega) = \frac{1}{\omega + i\eta}, \quad (15)$$

where η is a small quantity that controls the width of the δ function, namely, the imaginary part of $G^{(0)}$. We have assumed that the output of the nth iteration $G^{(n)}(\mathbf{k},\omega)$ has both real and imaginary parts $G^{(n)}(\mathbf{k},\omega) = G^{(n)}_R(\mathbf{k},\omega) + iG^{(n)}_I(\mathbf{k},\omega)$, where $G^{(n)}_R(\mathbf{k},\omega)$ and $G^{(n)}_I(\mathbf{k},\omega)$ are the results of the nth iterations of coupled equations derived from Eq. (14). The spectral function defined as

$$A(\mathbf{k},\omega) = -\frac{1}{\pi} G^{(\infty)}_I(\mathbf{k},\omega), \quad (16)$$

is obtained after the convergence for a given lattice size and given value of η is achieved.

III. VERTEX CORRECTIONS

Dyson's equation (14) has been obtained by considering only the self-energy diagrams without vertex correc-

tions. A fully dressed vertex contains diagrams due to the hole and spin-wave scattering, such as those shown in Fig. 1(a), where a solid line denotes the hole Green's function and a wavy line a spin-wave propagator. We find that the lowest-order vertex correction diagram shown in Fig. 1(b) gives zero contribution to the Green's function. To show this, let us write the dressed vertex as $\Gamma(\mathbf{k},\mathbf{q},\omega) = g(\mathbf{k},\mathbf{q})[1+\Lambda(\mathbf{k},\mathbf{q},\omega)]$. The vertex correction $\Lambda(\mathbf{k},\mathbf{q},\omega)$ due to the diagram of Fig. 1(b) can be written as

$$\Lambda(\mathbf{k},\mathbf{q},\omega) = \sum_{\mathbf{q}_1}[g^{-1}(\mathbf{k},\mathbf{q})g(\mathbf{k},\mathbf{q}_1)g(\mathbf{k}-\mathbf{q}_1,\mathbf{q})g(\mathbf{k}-\mathbf{q},\mathbf{q}_1)G(\mathbf{k}-\mathbf{q}_1,\omega-\Omega_{\mathbf{q}_1})G(\mathbf{k}-\mathbf{q}_1-\mathbf{q},\omega-\Omega_{\mathbf{q}_1}-\Omega_{\mathbf{q}})], \tag{17}$$

where the integration over the internal frequency has been carried out so that the spin wave propagator does not appear explicitly. Let us change variables in the summation over $\mathbf{q}_1$ such that $\mathbf{q}_1 \rightarrow \mathbf{q}_1 \pm (\pi,\pi)$ in the integrand of (17). The functions $g(\mathbf{k},\mathbf{q}_1)$ and $g(\mathbf{k}-\mathbf{q}_1,\mathbf{q})$ change sign, while $G(\mathbf{k}-\mathbf{q}_1,\omega)$ is invariant under this transformation as can be verified by Eq. (14). Thus, we find that $\Lambda(\mathbf{k},\mathbf{q},\omega) = -\Lambda(\mathbf{k},\mathbf{q},\omega)$ because there is an odd number of bare vertex functions having $\mathbf{q}_1$ as variable. Therefore, this vertex correction and all other diagrams, which are convolutions of $\Lambda(\mathbf{k},\mathbf{q},\omega)$, vanish. This implies that the only crossing two-loop self-energy diagram [Fig. 1(d)] is zero, and most two-loop vertex corrections contributing to the full vertex vanish; for example, among the eight diagrams shown explicitly in Fig. 1(a), only the first and eighth diagrams are nonzero.

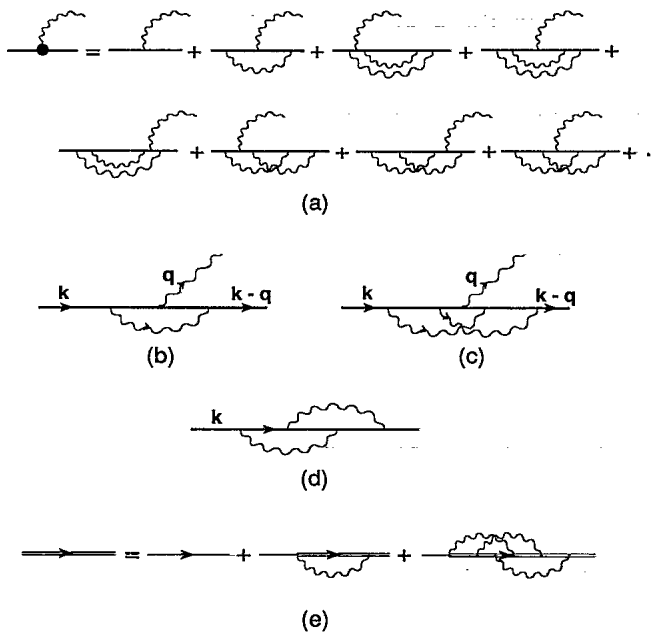

FIG. 1. (a) Diagrammatic contributions to the dressed vertex. The wavy line denotes a spin-wave propagator, while the solid line is the hole propagator. (b) The leading vertex correction (two-loop crossing diagram) is zero. (c) The leading nonzero vertex correction, which involves three loops. (d) The two-loop self-energy crossing diagram for zero. (e) Diagrammatic presentation of the Dyson's equation including all the three-loop crossing diagrams.

One can include the leading-order nonzero vertex correction diagram, shown in Fig. 1(c), in the Dyson's equation and solve it numerically. This self-consistent equation is shown diagrammatically in Fig. 1(d), where the solid line refers to the noninteracting Green's function as expressed in Eq. (15), while the double solid line denotes the hole propagator. This equation is solved self-consistently to find $G(\mathbf{k},\omega)$. In Figs. 2(a) and 2(b) we show the spectral function for $\mathbf{k} = (\frac{\pi}{2},\frac{\pi}{2})$ obtained on a 4^2 lattice for $J/t = 0.1$ and $J/t = 0.2$, respectively. The solid line denotes the one obtained using Eq. (14), and the dotted line is the one calculated self-consistently including all the three-loop crossing diagrams as illustrated by Fig. 1(d). The spectral function calculated on a 8^2 lattice for $t/J = 0.1$ is shown in Fig. 3. Notice that in all cases the lowest-energy peak, which is referred to as the quasiparticle peak, changes very little due to vertex corrections. Thus the dynamical properties of the quasiparticle will not be altered significantly by including vertex corrections. The influence of the vertex corrections on the peaks other than the lowest peak, however, is noticeable; generally speaking, the other peaks become better defined (sharper) when vertex corrections are introduced. The spectral function as a whole does not show any new structures on the 8^2 lattice by including these vertex corrections. Thus, we will perform our calculations in the following sections by neglecting vertex corrections.

We believe that the contribution of the three-loop crossing diagrams is small because of the following crude

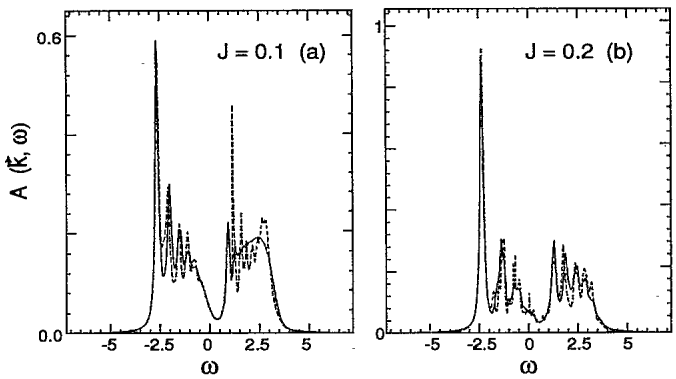

FIG. 2. (a) $A(\mathbf{k} = (\frac{\pi}{2},\frac{\pi}{2}),\omega)$ calculated on a 4^2 lattice for $J/t = 0.1$. The solid line represents the result obtained without any vertex corrections, while the dashed line denotes the solution obtained by including all the three-loop crossing diagrams. (b) The same as (a) for $J/t = 0.2$

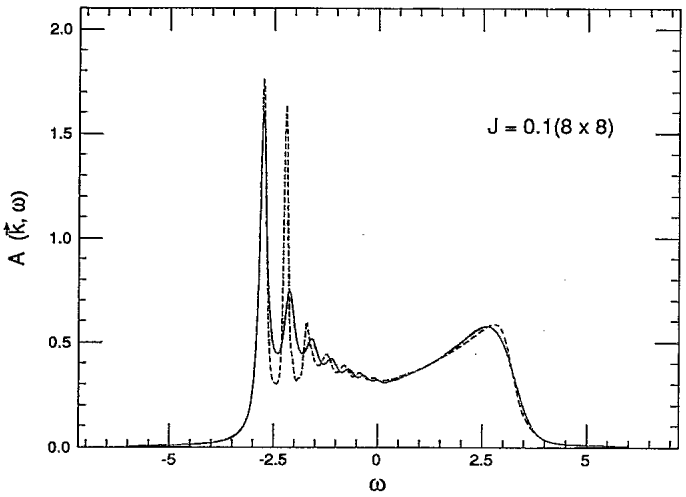

FIG. 3. The same quantities as Fig. 2(a) calculated on an 8^2 lattice.

argument. As suggested by KLR,[7] the dressed Green's function is of order $1/t$ (because the bare vertices are of order t, as indicted by Eq. (12) and the residue of the quasiparticle peak is of order J/t). Since the number of additional bare vertices and the number of internal hole Green's functions are the same, the three-loop crossing diagram at first sight is of order 1. However, every bare vertex also contributes a factor of $(u_q\gamma_{\mathbf{k}-\mathbf{q}} + v_q\gamma_{\mathbf{k}})$, whose absolute value is never larger than one. For the three-loop diagram shown in Fig. 1(c), the vertex correction $\Lambda(\mathbf{k},\mathbf{q},\omega)$ contains four such factors whose product thereby is very small. There is another crude argument, which may also be used to support this conclusion. As in the loop expansion treatment of the Heisenberg model,[2] where each loop contributes $1/z$, we also expect the same order of magnitude for each loop in this perturbation expansion. Therefore, the order of the three-loop crossing diagram is $1/z^3$. Thus, the vertex corrections give a small contribution at small J/t. At large J/t, however, the linearization of the original Hamiltonian is no longer a good approximation, and in particular the hopping part cannot be correctly described by (11).

IV. COMPARISON WITH EXACT RESULTS

In this section, we give our numerical results on a 4×4 cluster in order to compare with those obtained by means of the exact numerical diagonalization method on the same size cluster[11] to check the validity of this perturbation approach. We compare the spectral functions, the hole energy band, the quasiparticle bandwidth, and the spectral weight for various values of J/t. We find good agreement in the region $J/t \leq 0.2$.

In Fig. 4, we compare our results (solid lines) for $A(\mathbf{k},\omega)$ at $\mathbf{k} = (\frac{\pi}{2}, \frac{\pi}{2})$ calculated on a 4^2 lattice for typical values of J with the results of Dagotto *et al.*[11] (dotted lines) using the same value of η (we use units in which $t = 1$). We find several common features in the spectral functions between the two calculations. There exist a sharp quasiparticle peak at the bottom of the spectrum and also some fine structures above it. The agreement is good for small values of J, as shown in Fig. 4(c), where the quasiparticle peak and the second peak just above it almost overlap in the two calculations. There is also a pseudogap[11] around $\omega = 0$ in the case of $J = 0.2$ separating the negative from the positive energy peaks. The positive frequency spectrum, however, is somewhat different even in the small J region. There are four positive frequency peaks in both calculations but they are in different locations. We will argue in the next section

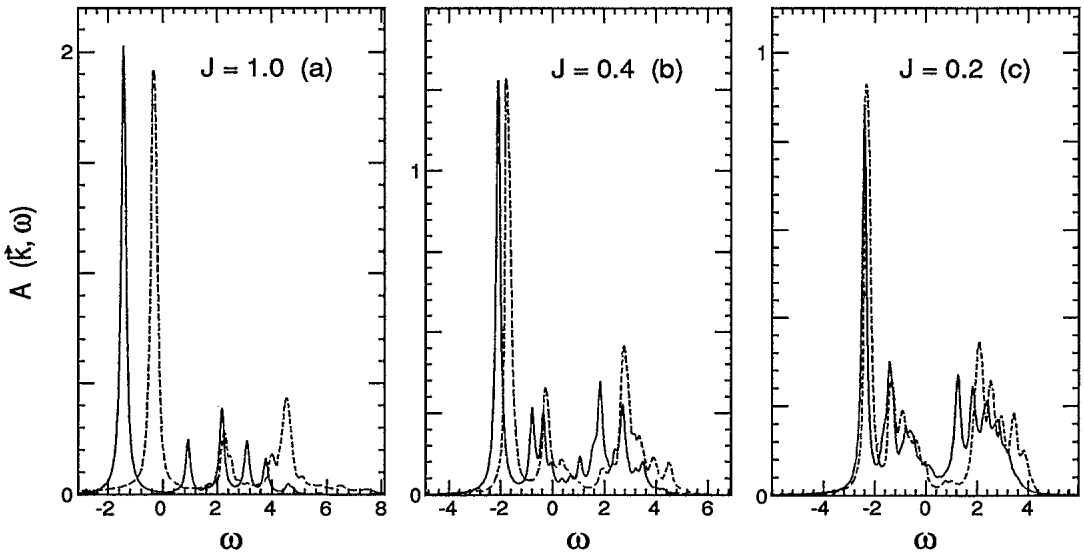

FIG. 4. The solid lines represent $A(\mathrm{k} = (\frac{\pi}{2}, \frac{\pi}{2}), \omega)$ calculated on a 4^2 lattice for typical values of J using $\eta = 0.1$. The dashed lines correspond to those shown in Fig. 5 of the paper by Dagotto *et al.*[11] Note that the agreement is good for small values of J, while for large J the locations of the peaks are at significantly different energies.

that most of these positive frequency peaks are replaced by a featureless incoherent band for large-size lattices and hence are caused by finite-size effects. The general agreement is poor for large J, as shown in Fig. 4(a) for $J = 1.0$, where the location of the quasiparticle peak is at significantly different energy from the exact calculation.

In Table I, the hole energies, the spectral weights of the lowest-energy peaks at $\mathbf{k} = (\frac{\pi}{2}, \frac{\pi}{2})$ and the quasiparticle bandwidths obtained on a 4^2 lattice for different J's are compared. The energy $E(\mathbf{k})$ of the hole state with respect to the no-hole ground state is obtained from the position of the lowest-frequency peak in the spectral function. The same definition was also used in extracting the hole energy in the exact diagonalization.[11] We have used $\eta = 0.1$ and $\Delta\omega = 0.004$. The quantity $\Delta\omega$ is the interval used in discretizing the energy range in order to solve Dyson's equation numerically. Errors introduced from this discretization are discussed in the next section. Our results of the quasiparticle energies at $\mathbf{k} = (\frac{\pi}{2}, \frac{\pi}{2})$ can be fit with a power law as $E(\frac{\pi}{2}, \frac{\pi}{2}) = -3.20 + 1.82J^{0.50}$, in the region of $0.02 \leq J \leq 0.4$. Comparison with the fit to the exact data, $E(\frac{\pi}{2}, \frac{\pi}{2}) = -3.17 + 2.83J^{0.73}$, obtained by Dagotto *et al.* is shown in Fig. 5. A good agreement exists in the narrow region $0 \leq J \leq 0.2$. Our result are consistent with the fact that this perturbation approach is valid in the small-J limit. Comparison of the same quantities plotted in Fig. 3 of Ref. 16, however, shows that the agreement is poor in both small and large J regions, except around the tiny region of $J \sim 0.55$. This is due to the fact that the definition of the Heisenberg exchange parameter J in Ref. 16 is different from that used by Dagotto *et al.* in Ref. 11.

The quasiparticle spectral weights have been calculated in our calculation using the formula

$$Z(\mathbf{k}) = \left(1 - \frac{\partial}{\partial\omega} Re\,\Sigma(\mathbf{k},\omega)\right)^{-1}\Big|_{\omega=E(\mathbf{k})}, \qquad (18)$$

where the derivative of the real part of the self-energy Σ with respect to ω is evaluated at $E(\mathbf{k})$, which is the position of the quasiparticle peak. This formula is a good approximation only when the peak is very narrow, namely, the imaginary part of the pole is close to zero. We have used values of $\eta = 0.1$ and $\Delta\omega = 0.006$ in obtaining the value of $Z(\frac{\pi}{2}, \frac{\pi}{2})$ in Table I in order to compare to the exact results.

TABLE I. The energy, residue, and bandwidth of the quasiparticle peak at $\mathbf{k} = (\frac{\pi}{2}, \frac{\pi}{2})$ calculated using a 4^2 lattice. The results obtained by exact diagonalization are shown in the parentheses for comparison in order to test the range of validity of the present method.

J	$E(\frac{\pi}{2}, \frac{\pi}{2})$	$Z(\frac{\pi}{2}, \frac{\pi}{2})$	W
0.10	−2.640(−2.643)	0.23(0.20)	0.248
0.20	−2.388(−2.298)	0.30(0.28)	0.448(0.271)
0.30	−2.208(−1.997)	0.36(0.35)	0.612(0.478)
0.40	−2.058(−1.722)	0.41(0.40)	0.748(0.667)
0.55	−1.872(−1.344)	0.49(0.46)	0.960(0.894)
0.70	−1.712(−0.993)	0.54(0.51)	0.976(1.038)
1.00	−1.448(−0.345)	0.64(0.59)	1.016(1.194)

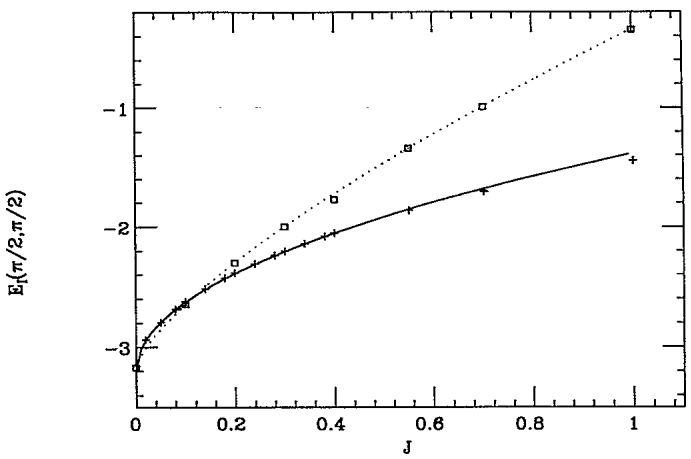

FIG. 5. The hole energy at momentum $\mathbf{k} = (\frac{\pi}{2}, \frac{\pi}{2})$ as a function of J on a 4^2 lattice. The crosses are our results and the solid line is our fit for $J \leq 0.4$. The squares are the exact results with a fit denoted by the dotted line taken from Ref. 11.

The quasiparticle band can be calculated from the energy of the lowest peak as a function of $\mathbf{k}$. The hole bandwidth W is defined as the difference between the hole minimum energy and maximum energy $W = E(0,0) - E(\frac{\pi}{2}, \frac{\pi}{2})$. The values of W obtained on a 4^2 lattice for different values of J are also given in Table I.

We have also calculated the energies of the lowest-energy peaks on the 4^2 lattice for different values of J and $\mathbf{k}$ (see the results in Table II). We find that the states $\mathbf{k} = (0,0)$ and $\mathbf{k} = (\pm\pi, \pm\pi)$ are always degenerate in our calculation, which is not true in the exact diagonalization study. For the 4^2 lattice, the hole ground state is a degenerate state with momenta $\mathbf{k} = (\pm\frac{\pi}{2}, \pm\frac{\pi}{2})$, $(\pi, 0)$, and $(0, \pi)$. The same degeneracy also exists in the exact hole ground state.[11] Nevertheless, this degeneracy is partially lifted for larger size lattices and, as we will see in the next section, the hole ground state always has momentum $\mathbf{k} = (\pm\frac{\pi}{2}, \pm\frac{\pi}{2})$ for those lattices in which such momentum states exist.

V. NUMERICAL RESULTS ON LARGE SIZE LATTICES

A. Finite-size effects

In order to study the hole spectral function, ideally one needs to take the limit $\Delta\omega \to 0$ first, then $N \to \infty$, and finally the limit $\eta \to 0$.

First we consider fixed values of N and η, and we decrease $\Delta\omega$ until convergence is achieved. The error in $A(\mathbf{k},\omega)$ is due to the propagation of the uncertainty of ω because ω is known only within $\pm\Delta\omega$. Let us, for the sake of our following discussion, define $Z(\omega)$ as the function given by the expression (18) at an arbitrary value of ω. We have found that by decreasing $\Delta\omega$ the value of Z at a given value of ω changes insignificantly. The most significant error in determining $Z(\omega = E(\mathbf{k}))$ (due to $\Delta\omega \neq 0$) is due to the fact that the value $E(\mathbf{k})$ of ω at

TABLE II. The hole energies calculated on a 4^2 lattice for different momenta are compared to those obtained by exact diagonalization (given in parentheses).

k	$J=0.2$	$J=0.4$	$J=0.7$	$J=1.0$
(0,0)	−1.950(−2.028)	−1.302(−1.055)	−0.684(0.045)	−0.390(0.849)
$(\frac{\pi}{2},0)$	−2.232(−2.135)	−1.836(−1.461)	−1.464(−0.648)	−1.218 (0.043)
$(\frac{\pi}{2},\frac{\pi}{2})$	−2.388(−2.298)	−2.052(−1.722)	−1.704(−0.993)	−1.446(−0.345)
$(\frac{\pi}{2},\pi)$	−2.232(−2.197)	−1.836(−1.582)	−1.464(−0.856)	−1.218(−0.236)

the maximum of the spectral function can only be determined within $\pm\Delta\omega$. Thus, by calculating the following quantity,

$$\epsilon(\omega)=\left|\frac{Z(\omega)-Z(\omega+\Delta\omega)}{Z(\omega)}\right|, \tag{19}$$

in the neighborhood of the peak we can obtain the magnitude of the error in $Z(E(\mathbf{k}))$ due to the finite value of $\Delta\omega$. In Table III, we give $Z(\frac{\pi}{2},\frac{\pi}{2})$ calculated for various values of N and η. These values have been obtained with $\Delta\omega=0.0006$ which introduces an error of $\bar{\epsilon}<1\%$ for $Z(\frac{\pi}{2},\frac{\pi}{2})$ [$\bar{\epsilon}$ is the average of $\epsilon(\omega)$ in the neighbor of the peak]. This value of $\Delta\omega$ implies 20 000 points in the ω interval $(-6\le\omega\le 6)$ and for a 24^2 lattice it requires about 12 megawords to save the real and imaginary part of the Green's function. We have restricted ourselves to accuracy of the order of 1% or less in the results reported next.

For a given value of η we need to increase the size of the lattice until convergence is achieved. As can be seen from Fig. 6(a) for small enough η the finite-size corrections to $Z(\frac{\pi}{2},\frac{\pi}{2})$ are of the order of $1/L$. The extrapolated values to the infinite square lattice are shown in Table III for small values of η.

Finally, we can study $Z(\frac{\pi}{2},\frac{\pi}{2})$ ($N\to\infty,\Delta\omega\to 0$) as a function of η. We have found that the finite η corrections to $Z(\frac{\pi}{2},\frac{\pi}{2})$ are of order η^2 and it is demonstrated in Fig. 6(b). The value of $Z(\frac{\pi}{2},\frac{\pi}{2})$ extrapolated to $\eta\to 0$ is identical to that obtained using $\eta=0.01$ within our acceptable error of 1%. Thus, the finite η corrections are negligible for $\eta\le 0.01$ and insensitive to our empirically chosen extrapolation form (i.e., $\sim\eta^2$).

In Fig. 7, we demonstrate the dependence of the entire $A(\mathbf{k},\omega)$ on the size of the lattice. It is clear (within the accuracy of the drawing) that all the other features of $A(\mathbf{k},\omega)$ have converged for lattices of sizes larger than 16^2. It is also shown in Fig. 7 that some features in the hole spectral function are changed due to finite-size effects. The pseudogap located for values of ω between 0 and 2 in Fig. 4(c) and the positive frequency peaks found in the exact diagonalization also appear in our calculation for 4^2 lattice [see the solid line in Figs. 4(c) and 7(a)]. However, as shown in Fig. 7 the pseudogap is replaced by some degree of depletion, and the positive frequency peaks are replaced by a featureless incoherent band in the lattices of 8^2 or larger. To give a further comparison, we show the spectral function in the small-J limit in Fig. 8 for 4^2 and 16^2 lattices. Again, the pseudogap that appeared on the 4^2 lattice disappears on the 16^2 lattice. Another important feature that we find is that there is a series of well-defined peaks above the lowest-energy peak, whose intensities decrease with increasing energy (such as peaks labeled II and III in Fig. 7). These peaks, as seen from Fig. 7, change insignificantly in going from an 8^2 to a 32^2 lattice.

In Fig. 9 we show $A(\mathbf{k}=(\frac{\pi}{2},\frac{\pi}{2}),\omega)$ calculated on a 16^2 lattice using $\eta=0.005$ (solid line) and $\eta=0.01$ (dashed line) in order to study the scaling behavior of the peaks and their widths with respect to changes in η. The width of the lowest-energy peak is proportional to η; more precisely, it fits quite closely with a Lorentzian $(1/\pi)\{Z\eta/[(\omega-\omega_I)^2+\eta^2]\}$ (where $\omega_{\rm I}$ is the location of the first peak), which in the limit $\eta\to 0$ becomes $Z\delta(\omega-\omega_{\rm I})$. Thus the first peak corresponds to a well-defined excitation with long lifetime. This strong dependence of the first peak on η is demonstrated in the inset of Fig. 9. Namely, while the width at half peak is $\sim 2\eta$ and the height is $\sim\frac{Z}{\eta}$, the residue Z [the integral of $A(\mathbf{k},\omega)$ around the peak] remains nearly unchanged. In Fig. 9, we also see that, while the width of peak I (see the inset) is very sensitive to η, the widths of the other peaks change by a much smaller amount. We have found that the width at half peak of the second-lowest peak can be fit as $\Gamma_{\rm II}=0.163+3.33\eta$. The widths of the first- and second-lowest-energy peaks in the spectral function are shown in Fig. 10 as functions of η. Thus, this suggests

TABLE III. The residue $Z(\mathbf{k})$ of the lowest-energy peak for $\mathbf{k}=(\frac{\pi}{2},\frac{\pi}{2})$ and $J=0.2$ is given for several size lattices and values of η. The numbers in the last row are the values extrapolated to the infinite size lattice. A value of $\Delta\omega=0.0006$ has been used.

Size	$\eta=0.1$	$\eta=0.05$	$\eta=0.025$	$\eta=0.01$	$\eta=0.005$
4^2	0.299	0.286	0.282	0.281	0.281
8^2	0.274	0.251	0.246	0.244	0.244
16^2	0.277	0.241	0.229	0.226	0.225
20^2	0.279	0.241	0.226	0.222	0.221
24^2	0.280	0.241	0.225	0.220	0.219
∞^2			0.212	0.207	0.206

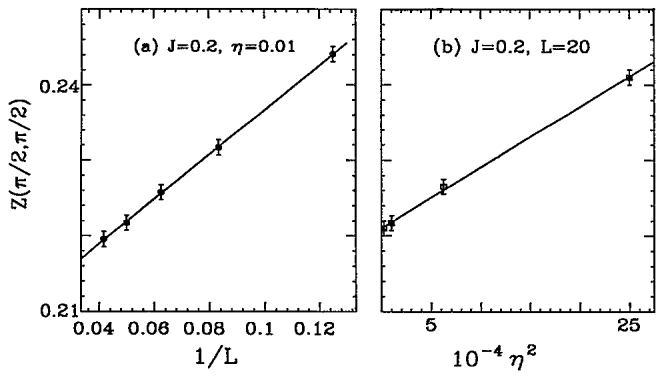

FIG. 6. (a) The finite-size corrections to the residue at $\mathbf{k} = (\frac{\pi}{2}, \frac{\pi}{2})$ of order $1/L$. (b) Demonstration that with our definition of $Z(\mathbf{k})$ [we use Eq. (18) with the derivative calculated at the peak of $A(\mathbf{k}, \omega)$] the finite-η corrections are of order η^2.

that the lowest-energy peak has a zero width, while the second- and the higher-energy peaks have finite widths.

It is interesting to study how the widths of the peaks change due to finite-size effects. In Fig. 11, we show the first- and second-lowest peaks calculated on 16^2 and 32^2 lattices and shown by the dashed and solid lines, respectively. Although the height and the shape of the first peak change somewhat, the widths are the same within our accuracy and they are both equal to 2η. The second peak shown in Fig. 11(b) calculated on the two-size lattices has the same width and shape; thus it strongly indicates that those peaks above the lowest peak are not due to finite-size effects, since they do not change by increasing the size of the lattice.

Thus, these additional peaks are not due to finite-size effects, and they survive the extrapolation limits $\eta \to 0$ and $N \to \infty$. We will discuss the origin of these additional peaks in Sec. V C.

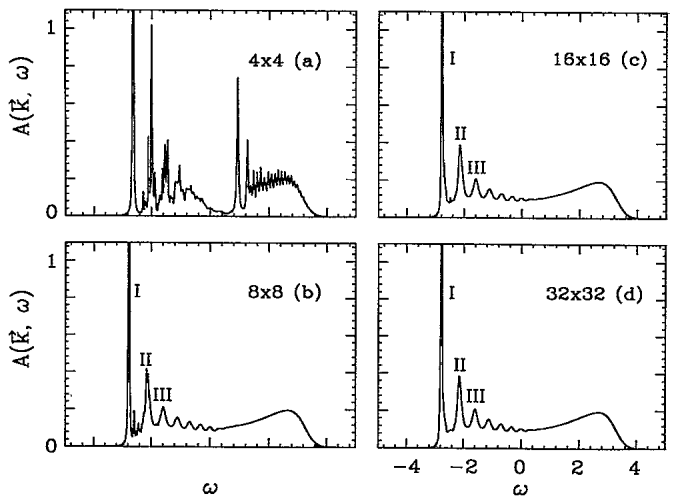

FIG. 7. $A(\mathbf{k} = (\frac{\pi}{2}, \frac{\pi}{2}), \omega)$ for $J = 0.1$ and $\eta = 0.01$. The results are obtained on 4^2, 8^2, 16^2, and 32^2 lattices.

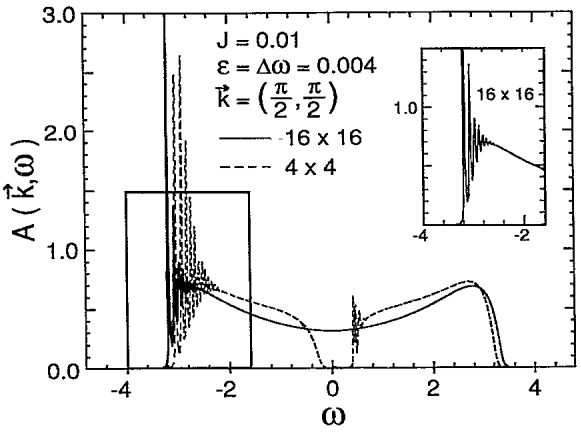

FIG. 8. $A(\mathbf{k} = (\frac{\pi}{2}, \frac{\pi}{2}), \omega)$ for $\eta = \Delta\omega = 0.004$, and $J = 0.01$. The dashed and solid lines denote the results on 4^2 and 16^2 lattices, respectively. The inset gives the spectral function for the larger-size lattice (16^2) in the region $-4 \leq \omega \leq -2$, where there is strong overlap with the results obtained on the 4^2 lattice.

B. Spectral functions and features of the quasiparticle state

The spectral function at $\mathbf{k} = (\frac{\pi}{2}, \frac{\pi}{2})$ is characterized by a large peak at the bottom of the spectrum and several other well-defined peaks above it. These features, however, are not universal for all the momentum states. In Fig. 12, we show the momentum dependence of the spectral function on a 32^2 lattice for $J = 0.2$. We find that for a wide range of J although the lowest-energy peak in the spectral function at $\mathbf{k} = (0, 0)$ is quite visible, it has a small spectral weight. The main peak is located at a

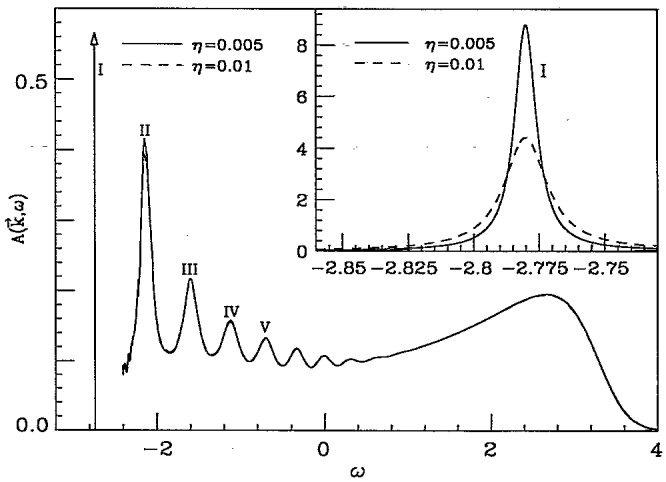

FIG. 9. $A(\mathbf{k} = (\frac{\pi}{2}, \frac{\pi}{2}), \omega)$ for $J = 0.1$ calculated on a 16^2 lattice. The solid and dashed lines denote the results obtained using $\eta = 0.005$ and 0.01, respectively. Because of the large difference in amplitudes and widths between the first and the other peaks, we have used two different scales. The first peak is only shown in the inset, while the rest of $A(\mathbf{k}, \omega)$ is shown in the main figure.

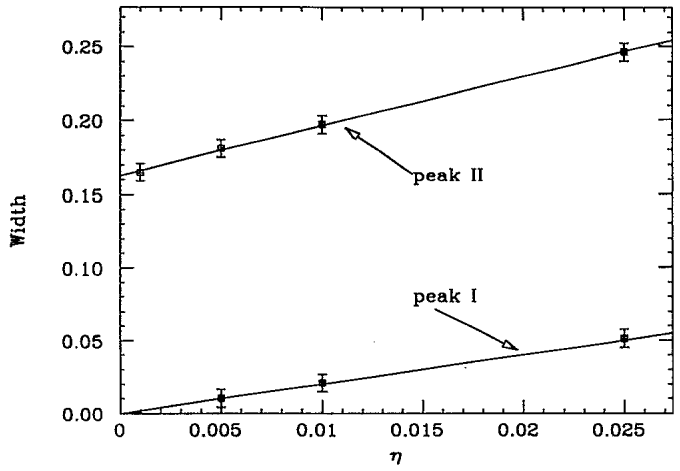

FIG. 10. The width of the first two lowest peaks of $A(\mathbf{k} = (\frac{\pi}{2}, \frac{\pi}{2}), \omega)$ obtained on a 16^2 lattice for $J = 0.1$ as a function of η.

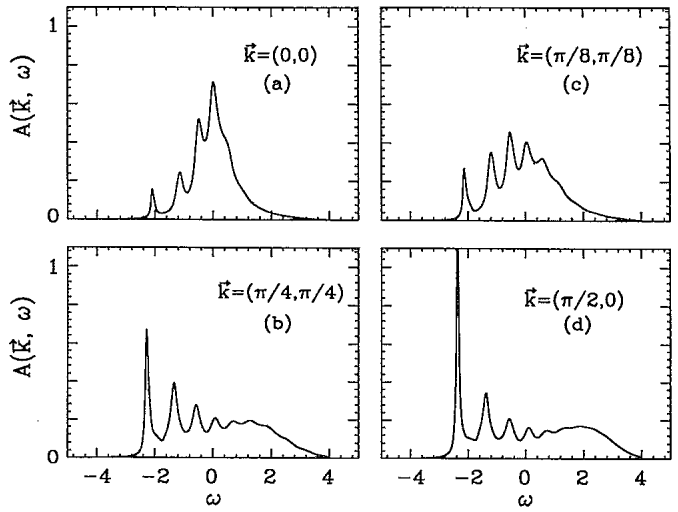

FIG. 12. The momentum dependence of the spectral function at $J = 0.2$. The results are obtained on a 32^2 lattice. The values of $\eta = 0.01$ and $\Delta\omega = 0.004$ have been used.

higher-energy position around $\omega = 0$. This indicates that there is not necessarily a large sharp quasiparticle peak forming at the bottom of the spectrum for all momentum states; this is in disagreement with the suggestion of KLR that there should be a large peak at the bottom of the spectrum due to the small density state of spin waves. The spectral function at $\mathbf{k} = (0,0)$ calculated on the 4^2 lattice by exact diagonalization studies[11] also shows a lowest-energy peak with tiny spectral weight for a wide region of J. The similarity between the two calculations may be regarded as another support for the validity of this perturbation approach.

The minimum of the hole band is found with the present method to be at $\mathbf{k} = (\pm\frac{\pi}{2}, \pm\frac{\pi}{2})$. The hole band has very similar features to those found by other calculations,[7–12,14] namely, an anisotropic effective mass with a large value in the direction of the Brillouin zone $(\pi,0)$–$(0,\pi)$ and a small value in the direction $(0,0)$–(π,π). The hole band $E(\mathbf{k})$ is computed on a lattice 32^2 for $J = 0.2$ and shown along the path $\Gamma M X \Gamma$ (see the inset) of the Brillouin zone in Fig. 13. The bandwidth W, obtained on a 16^2 lattice, is shown in Fig. 14(a). The solid line is the difference of the forms $E(0,0) = -3.28 + 3.42J^{2/3}$ and $E(\frac{\pi}{2}, \frac{\pi}{2}) = -3.28 + 2.16J^{2/3}$ found by fitting $E(0,0)$ and $E(\frac{\pi}{2}, \frac{\pi}{2})$ as a function of J. The basis for these forms is discussed in Sec. V C.

The spectral weights of the quasiparticle peak for $\mathbf{k} = (\frac{\pi}{2}, \frac{\pi}{2})$ are calculated on the 20^2 lattice and given in Fig. 14(b). We have chosen $\eta = 0.01$ and $\Delta\omega = 0.0006$ in our calculation. The solid line is our fit $Z(\frac{\pi}{2}, \frac{\pi}{2}) = 0.65J^{0.67}$ in the region $0.05 \leq J \leq 0.4$. These data can be fit nicely for a wide region of J by an approximate square root function of J but with a small unphysical negative intercept.

In Fig. 15, we show the tunneling density of states for removing a particle defined as $D(\omega) = \sum_{\mathbf{k}} A(\mathbf{k}, \omega)$, which has been calculated on a 32^2 lattice for $J = 0.2$. The structure looks very similar to those of the spectral functions for momenta not close to the center of the Bril-

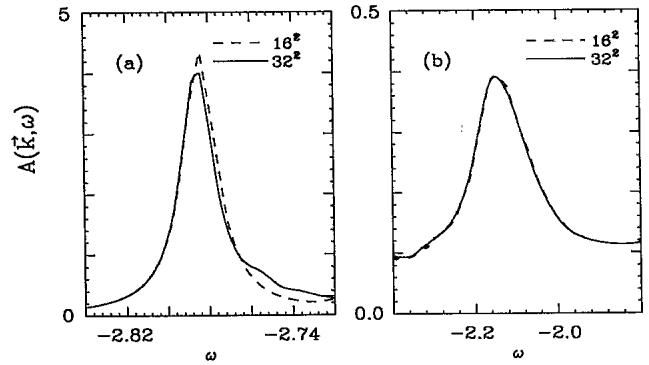

FIG. 11. The first- (a) and second- (b) lowest peaks of $A(\mathbf{k} = (\frac{\pi}{2}, \frac{\pi}{2}), \omega)$ for $J = 0.1$ and $\eta = 0.01$. The dashed and solid lines are the results obtained using the 16^2 and 32^2 lattices, respectively.

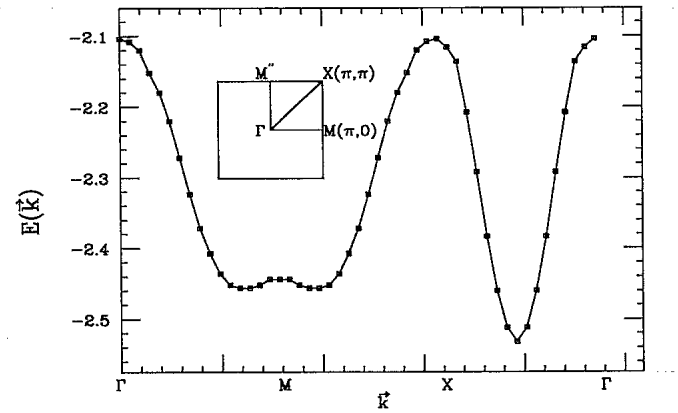

FIG. 13. The hole dispersion curve, plotted along the direction $\Gamma M X \Gamma$ in the Brillouin zone (see inset), for a 32^2 lattice, for $J = 0.2$.

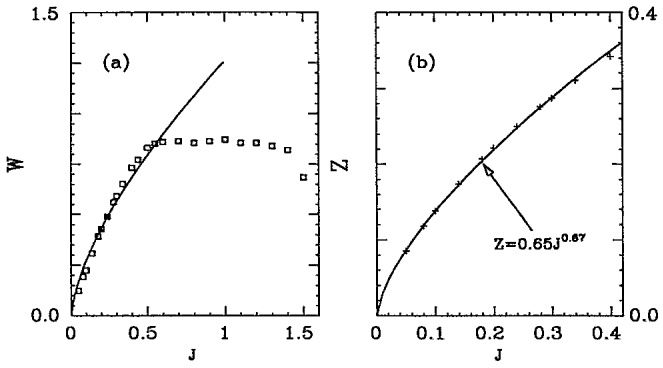

FIG. 14. (a) The hole bandwidth W, as a function of J for a 16^2 lattice. The solid line is our fit for $J \leq 0.2$ (see text). (b) The spectral weight $Z(\frac{\pi}{2}, \frac{\pi}{2})$ of the lowest-energy peak, as a function of J for a 20^2 lattice. The solid line is the fit for $J \leq 0.4$ to the function shown in the figure.

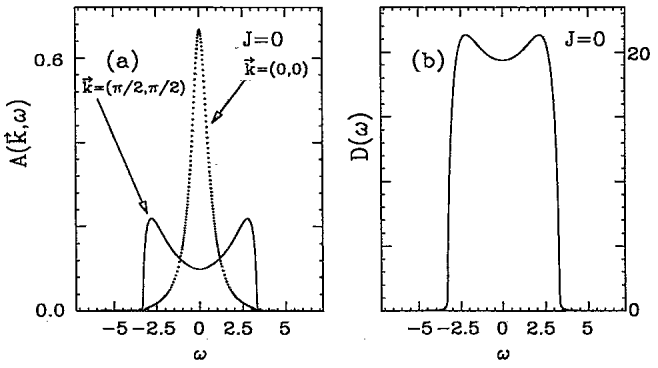

FIG. 16. The results in the $J = 0$ limit on a 16^2 lattice. The values of $\eta = 0.01$ and $\Delta\omega = 0.006$ have been used. (a) The spectral functions for $\mathbf{k} = (\frac{\pi}{2}, \frac{\pi}{2})$ and $\mathbf{k} = (0, 0)$ are denoted by a solid line and a dotted line, respectively. (b) The tunneling density of states for $J = 0$.

louin zone, as shown in Figs. 12(b) and 12(d) because of the large density of states around the boundary of the Brillouin zone corresponding to one sublattice.

The distinction between the states near $\mathbf{k} = (0, 0)$ and other momentum states exists even for the limiting case of $J = 0$. In Fig. 16(a), we show the spectral function calculated on the 16^2 lattice in this limit for $\mathbf{k} = (\frac{\pi}{2}, \frac{\pi}{2})$ (solid line) and $\mathbf{k} = (0, 0)$ (dotted line). This result is different from that obtained on the Hubbard model in the infinite-U limit, where a momentum-independent spectral function was found.[4] The spectral function would have had a sharper band edge if the value of η smaller than 0.01 were used. It is difficult, however, to achieve convergence using such a small value of η. The tunneling density of states in the $J = 0$ limit is also shown in Fig. 16(b). From Fig. 16, we can approximately determine that the band edge is at $\omega_0 \sim -3.3$, which is close to $-2\sqrt{z-1}$ obtained by Brinkman and Rice[4] in the limit of $J = 0$. Thus, $A(\mathbf{k}, \omega)$ has $\mathbf{k}$ dependence in the $J \to 0$ limit if one keeps the isotropic nature of the J term. The results would be different if we set $J_\perp \to 0$ first and then take the limit $J_z \to 0$. Namely, $A(\mathbf{k}, \omega)$ obtained from the t-J_z model has no $\mathbf{k}$ dependence, $A(\omega) = (2\pi z t^2)^{-1/2}(4zt^2 - \omega^2)^{1/2}$ within this approach.[7] It is important to keep in mind this nonanalytic behavior as $J \to 0$. The spin-wave excitations in the isotropic t-J model with only one hole have no gap and the excitation spectrum is linear in momentum, i.e., $\omega(k) \to ck$ as $k \to 0$. On the contrary, for small but finite J_z there is a finite gap in the t-J_z model. Another way that the nonanalyticity of the $J \to 0$ limit manifests itself is in the expression of the J dependence for the hole ground state and the excitations of this model, which is discussed in the next part.

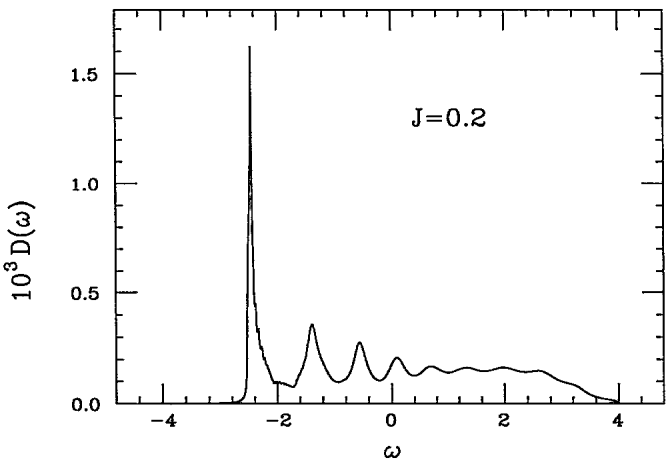

FIG. 15. Tunneling density of states for $J = 0.2$ on a 32^2 lattice.

In Table IV, we give the numerical values of the hole ground-state energy, spectral weight, and bandwidth for different values of J calculated on a 20^2 lattice. We have found by examining the size dependence of the energy $E(\mathbf{k})$ that at $\mathbf{k} = (\frac{\pi}{2}, \frac{\pi}{2})$ the finite-size corrections are of order of $1/N$. The finite-size corrections to $Z(\frac{\pi}{2}, \frac{\pi}{2})$ are of order of $1/L$ as shown in the previous part. The values obtained by extrapolation (using $8^2, 12^2, 16^2$, and 20^2 lattices) are shown by the numbers in parentheses in the table. Notice that the finite-size effects on the energy calculated on a 20^2 lattice are insignificantly small, while those on the residue $Z(\frac{\pi}{2}, \frac{\pi}{2})$ are somewhat larger.

TABLE IV. The energy, residue and bandwidth of the quasiparticle peak at $\mathbf{k} = (\frac{\pi}{2}, \frac{\pi}{2})$ calculated using a 20^2 lattice. The numbers in the parentheses are the values extrapolated to the infinite size lattice. The value of $\eta = 0.01$ and $\Delta\omega = 0.0006$ have been used.

J	$E(\frac{\pi}{2}, \frac{\pi}{2})$	$Z(\frac{\pi}{2}, \frac{\pi}{2})$	W
0.10	−2.782(−2.786)	0.138(0.123)	0.237
0.20	−2.543(−2.548)	0.222(0.202)	0.424
0.30	−2.362(−2.367)	0.287(0.271)	0.600
0.40	−2.212(−2.217)	0.342(0.325)	0.748
0.55	−2.021(−2.026)	0.411(0.392)	0.888
0.70	−1.859(−1.864)	0.464(0.446)	0.955
1.00	−1.591(−1.595)	0.570(0.533)	0.963

C. The string picture

In this part we further study the distinct peaks in the spectral function lying above the lowest-energy peak, which have already been discussed in Sec. V A. Similar peaks have also been found by Dagotto *et al.*[11] in the exact diagonalization on a 4^2 lattice.

As already mentioned, these additional peaks in our spectral function are not due to finite-size effects. In particular, in Fig. 7, we have demonstrated that by changing the size of the system from 8^2 to 32^2 neither the heights nor the width of the second, third, etc., peaks change. In addition, by changing η we show that these peaks survive the limit $\eta \to 0$. It is clear that these peaks exist in the limit $\Delta\omega \to 0, \eta \to 0$, and $N \to \infty$. In Figs. 17(a)–17(c), we show $A(\mathbf{k} = (\frac{\pi}{2}, \frac{\pi}{2}), \omega)$ calculated on a 32^2 lattice. It is shown how those secondary peaks change by increasing J from the value $J = 0.1$ in Fig. 7 to $J = 0.2$, 0.3, and 0.4 in Fig. 17. Thus, our calculation shows that above the lowest-energy peak the spectrum is not incoherent as assumed in the dominant-pole approximation by KLR (Ref. 7), but also has a series of other peaks.

We will try to understand these peaks in terms of the so-called string picture. For illustration, let us consider a special case, namely, a single hole moving in a Néel spin background. The Hamiltonian describing the hole motion in this case is usually called the t-J_z model. As the hole moves, it displaces antiferromagnetically aligned spins and causes a string of overturned spins. Thus, the further a hole hops, the higher the energy costs to create more overturned spins. For small values of J_z, the hole "sees" a linear potential.[8] The J_z dependence of the hole eigenvalues has the following power-law behavior:

$$E_n/t = -2\sqrt{3} + a_n(J_z/t)^{2/3}, \tag{20}$$

where a_n are the eigenvalues of a dimensionless Airy equation.[7] This equation gives a quantitative description for the characteristics of string excitations.

In this section we will show that for various momentum states the energies of the first three lowest energy peaks can be fit by functions of J/t which have a power-law behavior as suggested by Eq. (20). We argue that a string excitation, which describes the hole low-energy levels as it moves in Néel spin background, may also be true for the small-J case even though quantum spin fluctuations exist in the Heisenberg antiferromagnet. Although this conclusion was drawn earlier by Trugman[10] using a variational method for some chosen spin configurations and by Dagotto *et al.*[11] using Lanczos techniques on 4^2 lattice, our analysis in this section, based on the results obtained on larger-size lattices, provides a strong support for the string description of the hole excitations. In addition, we have performed a rather convincing analysis that these peaks survive the extrapolation limits (infinite size lattice, broadening parameter $\eta \to 0$).

In order to find the J dependence of the positions of these peaks, we carry out the calculation on a 16^2 lattice, and in Fig. 18 we show the energies for different J for the first three lowest-energy peaks [the peaks labeled I, II, and III in Fig. 17(a)]. To compare these three peaks with the energies of the "string" excitations in the t-J_z model given by Eq. (20), we fit our data with the functions $a + b_n J^{2/3}$ and treat a, b_1, b_2, and b_3 as fitting parameters (we remind the reader that we use units of $t = 1$). We use a common fitting parameter a for all the three peaks because they should shrink to the same value in the $J \to 0$ limit. The locations of the first three peaks are best fit to the forms $E_{\rm I} = -3.28 + 2.16J^{2/3}$, $E_{\rm II} = -3.28 + 5.46J^{2/3}$, and $E_{\rm III} = -3.28 + 7.81J^{2/3}$ in the region of $0.02 \le J \le 0.4$, and in Fig. 18 they are denoted by a dashed line, a solid line, and a dotted line, respectively. Because these three peaks are well defined even for very small values of J, we are able to fit our data starting from a small value of $J = 0.02$ up to $J = 0.4$. These fits are very good with fewer fitting parameters so we avoided using the exponents as fitting parameters for simplicity. Recalling the solutions for the Airy equation, a_n=2.33, 4.08, and 5.52 corresponding to the first three peaks, our three fitting functions are somewhat close to these of Eq. (20) describing the string excitations in the

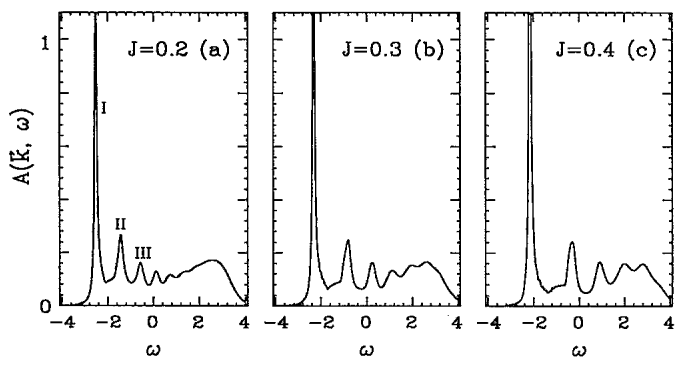

FIG. 17. The spectral functions at $\mathbf{k} = (\frac{\pi}{2}, \frac{\pi}{2})$ obtained on a 32^2 lattice for different values of J.

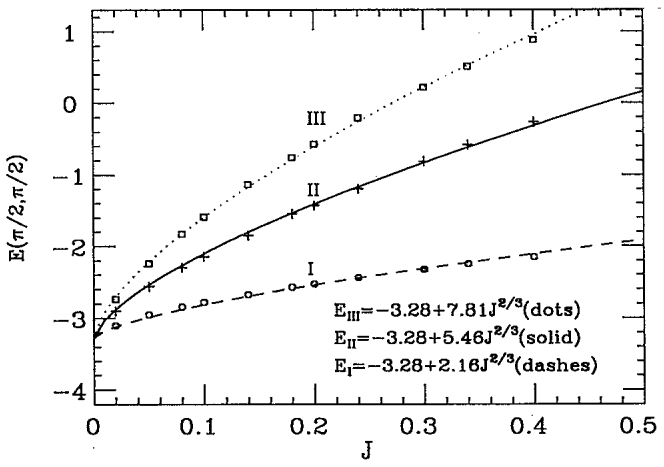

FIG. 18. Energies of the first three lowest-energy levels for $\mathbf{k} = (\frac{\pi}{2}, \frac{\pi}{2})$ as a function of J on a 16^2 lattice. The circles denote the energies of the first peak and the dashed line is the fit to these data by the functions given in the figure. The crosses and squares refer to the second and third peaks, and solid and dotted lines are the fitting functions. We have used $\eta = 0.01$ and $\Delta\omega = 0.004$.

t-J_z model. The band edge obtained from the fitting function is -3.28, which is very close to that extracted from our numerical solutions of the spectral function in the $J = 0$ limit shown in Fig. 16. Notice that the point $J = 0$ is a singular point of our fitting functions $E_n(J)$. This tells us that a perturbation treatment, where the expansion parameter is J, does not converge. As discussed in Sec. V B, a singular behavior was detected in $A(\mathbf{k},\omega)$ in the limit $J \to 0$. In this limit of the isotropic t-J model, $A(\mathbf{k},\omega)$ is $\mathbf{k}$ dependent and has a band edge $\omega_0 \sim -3.3$, which is different from that obtained by taking the $J_\perp \to 0$ limit first, and the $J_z \to 0$ limit afterwards.

To study the string states for different momenta, we have also calculated the J dependence for the first three lowest-energy peaks for $\mathbf{k} = (\frac{\pi}{2},0)$ and $(0,0)$. Using the same fitting scheme mentioned above, we obtain the following results. For $\mathbf{k} = (\frac{\pi}{2},0)$, we find that the first three lowest-energy peaks can be fit by $E_{\rm I} = -3.27 + 2.69J^{2/3}$, $E_{\rm II} = -3.27 + 5.44J^{2/3}$, and $E_{\rm III} = -3.27 + 7.94J^{2/3}$ in the region of $0.02 \le J \le 0.2$. In the same region of J, for $\mathbf{k} = (0,0)$, we find $E_{\rm I} = -3.28 + 3.42J^{2/3}$, $E_{\rm II} = -3.28 + 6.29J^{2/3}$, and $E_{\rm III} = -3.28 + 8.40J^{2/3}$. The quality of these fits is the same as in the case of $\mathbf{k} = (\frac{\pi}{2},\frac{\pi}{2})$ (see Fig. 18).

The first five peaks above the lowest-energy peak can be well reproduced by the superposition of a series of Lorentzian functions, as shown in Fig. 19, where the solid line is the calculated spectral function and the dashed lines represent five Lorentzian functions, while the dotted line is the superposition of these five Lorentzian functions. We have used the Lorentzians $L_i(\omega) = (a_i\Gamma_i^2)/[(\omega-\omega_i)^2+\Gamma_i^2]$, where i runs from II to VI, to represent the five peaks and ω_i are the positions of the peaks. We used a_i and Γ_i as adjustable parameters. We find that the widths of these Lorentzians increase as the energy increases (e.g., for the first three peaks $\Gamma_i = 0.097, 0.158$, and 0.175). This tells us that the lifetime of these excitations decrease with energy as expected. For a higher-energy excitation of the hole in the nearly linear potential, the characteristic time [in a semiclassical treatment of the problem (e.g., WKB)] to reach the turning point of the linear potential is larger. Thus, during a longer period of oscillation the hole has better chances to "see" spin fluctuations taking place (i.e., time-dependent deviations from the linear potential), since the time scale for quantum spin fluctuations is of order $1/J$. In Fig. 20 we show the width of the second-lowest peak as a function of J. As expected, the excitations become longer lived in the limit $J \to 0$ because in the region of small J/t the time scale for spin fluctuations is much larger than that for hole hopping, so the width (i.e., the inverse of the hole lifetime) of the peaks that correspond to the string excitations becomes very small (see also Fig. 8).

Thus, we believe that these peaks correspond to the hole excitations moving in an approximate linear potential imposed by the antiferromagnetically ordered background.

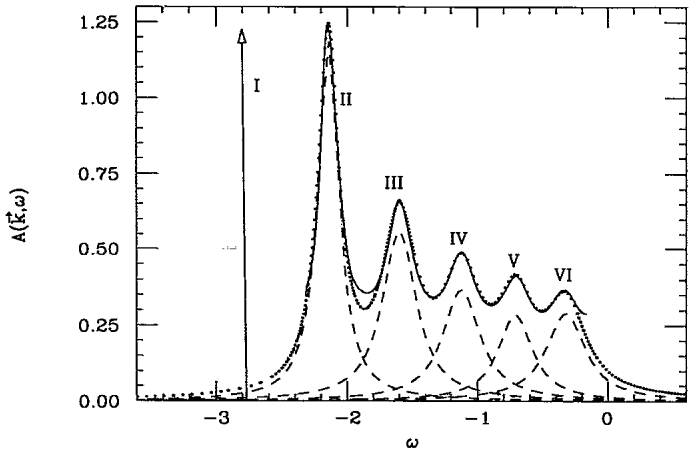

FIG. 19. The solid line shows the first five peaks above the lowest-energy peak of $A(\mathbf{k} = (\frac{\pi}{2},\frac{\pi}{2}),\omega)$ calculated on a 16^2 lattice for $J = 0.1$. The first peak is well outside the scale of this figure, and we only denote its location by the vertical arrow labeled I. The dashed lines represent five Lorentzian functions of $(a_i\Gamma_i^2)/[(\omega-\omega_i)^2+\Gamma_i^2]$. The dotted line is the superposition of these five Lorentzians.

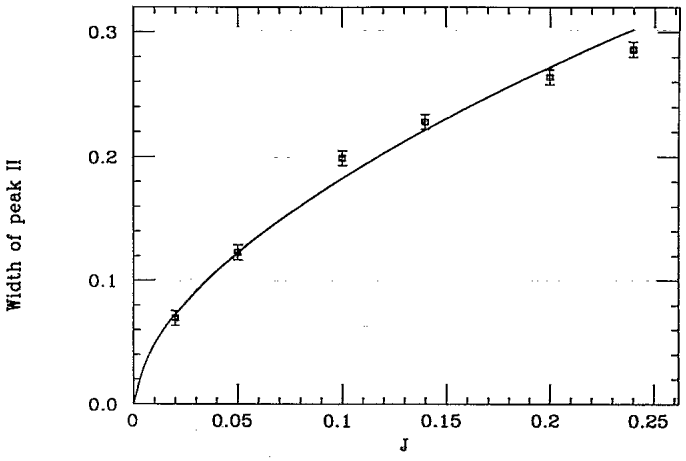

FIG. 20. The width of the second-lowest energy peak in $A(\mathbf{k} = (\frac{\pi}{2},\frac{\pi}{2}),\omega)$ calculated on a 16^2 lattice as a function of J. The line is a fit to the form $\Gamma_{\rm II} = 0.69J^{0.58}$.

VI. CONCLUSIONS

We have studied the dynamics of a hole in an ordered antiferromagnet within the t-J model in the large t/J limit by treating the spin-spin and spin-hole interactions in spin-wave approximation.[6,7] The hole motion is treated by a self-consistent perturbative scheme, which neglects crossing diagrams. A detailed numerical solution to the Dyson's equation for the single-hole Green's function has been obtained. Furthermore, we have studied the validity of this approximation, which ignores vertex corrections. We show analytically that the two-loop crossing diagrams are zero and the leading nonzero vertex correction is given by a three-loop crossing diagram. The numerical solutions show that the contributions of the three-loop crossing term to the spectral functions are small. In order to compare with the results obtained

by exact diagonalization we calculated the spectral function on a small size lattice (4^2), where there are available results. The comparison of our numerical results obtained by neglecting vertex corrections with those obtained by means of exact diagonalization method shows a close agreement in the parameter region $J/t \leq 0.2$. Therefore, we conclude that the difference between our results and those obtained by the exact diagonalization for larger J/t, is mainly due to the spin-wave approximation used to derive the effective Hamiltonian (6) and (11).

The convergence of the Dyson's equation can be easily achieved numerically on quite large-size lattices; we are able to estimate the finite-size effects and perform extrapolation to the infinite-size lattice. We found that our results for the larger size lattice used in our calculation are very close to the extrapolated values. A careful study of the effects of the finite broadening parameter η is carried out and the extrapolation to the $\eta \rightarrow 0$ limit is also studied.

Our study of the hole spectral functions for different momentum states shows that above the lowest-energy peak the spectrum is not incoherent but has a series of well-defined peaks, which survive in the thermodynamic limit. The positions of the first three lowest-energy peaks in the spectral function for various momentum states are well fit by $\sim -3.3 + b_n J^{2/3}$ in the region of small J/t. The analysis of our results shows that these peaks correspond to string excitations, which become better defined in the limit of small J/t. In that limit the time scale for spins to relax (via quantum fluctuations) is larger than the time scale for a hole to move by a few lattice spacings. Thus, the hole moves in an antiferromagnetically correlated background, and it sees an approximately linear potential arising from the string of overturned spins. Indeed, our numerical results suggest that the string excitations for a single hole also exist in the lightly doped t-J model in the small J/t region.

Finally, we wish to stress the fact that the $J = 0$ is a singular point of the phase diagram of the t-J model. In our calculation this manifests itself in the following two cases: (a) The nonanalytic dependence of the quasiparticle energies on J, namely, at small J, can be well approximated by $a + b_n J^{2/3}$. (b) The spectral function $A(\mathbf{k},\omega)$, of the t-J model in the limit $J \rightarrow 0$, is $\mathbf{k}$ dependent. This is different from the case of the t-J_z model in the limit of $J_z \rightarrow 0$.

ACKNOWLEDGMENTS

This work was supported in part by the Supercomputer Computations Research Institute, which is partially funded by the U.S. Department of Energy under Contract No. DE-FC05-85ER-250000.

[1] S. Chakravarty, in *High Temperature Superconductivity*, edited by K. S. Bedell, D. Coffey, D. E. Meltzer, D. Pines, and J. R. Schrieffer (Addison-Wesley, Reading, MA, 1990), p. 136.
[2] E. Manousakis, Rev. Mod. Phys. **63**, 1 (1991).
[3] F. C. Zhang and T. M. Rice, Phys. Rev. B **37**, 3759 (1988).
[4] W. Brinkman and T. Rice, Phys. Rev. B **2**, 1324 (1970).
[5] C. Gros and M. Johnson, Phys. Rev. B **40**, 9423 (1989).
[6] S. Schmitt-Rink, C. M. Varma, and A. E. Ruckenstein, Phys. Rev. Lett. **60**, 2793 (1988).
[7] C. Kane, P. Lee, and N. Read, Phys. Rev. B **39**, 6880 (1989).
[8] B. Shraiman and E. Siggia, Phys. Rev. Lett. **60**, 740 (1988); **61**, 467 (1988); V. Elser, D. Huse, B. Shraiman, and E. Siggia, Phys. Rev. B **41**, 6715 (1990).
[9] S. Sachdev, Phys. Rev. B **39**, 12 232 (1989); M. Boninsegni and E. Manousakis, *ibid.* **43**, 10 353 (1991).
[10] S. A. Trugman, Phys. Rev. B **37**, 1597 (1988); **41**, 892 (1990).
[11] E. Dagotto *et al.*, Phys. Rev. B **41**, 9049 (1990).
[12] K. J. von Szczepanski, P. Horsch, W. Stephan, and M. Ziegler, Phys. Rev. B **41**, 2017 (1990).
[13] E. Dagotto and J. R. Schrieffer, Phys. Rev. B **43**, 8705 (1991).
[14] B. Chakraborty *et al.*, Phys. Rev. B **42**, 4819 (1990); F. Nori, E. Abrahams, and G. Zimanyi, *ibid.* **41**, 7277 (1990); D. Poilblanc and E. Dagotto, *ibid.* **42**, 4861 (1990); Z. Zou and R. B. Laughlin, *ibid.* **42**, 4073 (1990); J. M. F. Gunn and B. D. Simons, *ibid.* **42**, 4370 (1990); T. Itoh *et al.*, *ibid.* **42**, 4834 (1990); J. R. Schrieffer, X. G. Wen, and S. C. Zhang, *ibid.* **39**, 11 663 (1989); R. Shankar, Phys. Rev. Lett. **63**, 203 (1989); S. A. Trugman, *ibid.* **65**, 500 (1990).
[15] Z. Liu and E. Manousakis, Phys. Rev. B **44**, 2414 (1991).
[16] F. Marsiglio, A. Ruckenstein, S. Schmitt-Rink, and C. Varma, Phys. Rev. B **43**, 10 882 (1991).
[17] G. Martínez and P. Horsch, Phys. Rev. B **44**, 317 (1991).
[18] P. W. Anderson, Phys. Rev. **86**, 694 (1952); R. Kubo, *ibid.* **87**, 568 (1952); T. Oguchi, *ibid.* **117**, 117 (1960).